Large exchange anisotropy in quasi-one-dimensional spin-$\frac{1}{2}$ fluoride antiferromagnets with a $d(z^2)^1$ ground state

D. Kurzydłowski[1,2,*] and W. Grochala[1,*]

[1]*Centre of New Technologies, University of Warsaw, Banacha 2c, 02-097 Warsaw, Poland*

[2]*Faculty of Mathematics and Natural Sciences, Cardinal Stefan Wyszyński University in Warsaw, Wóycickiego 1/3, 01-938 Warsaw, Poland*

(Received 28 April 2017; revised manuscript received 4 July 2017; published 26 October 2017)

Hybrid density functional calculations are performed for a variety of systems containing d^9 ions (Cu^{2+} and Ag^{2+}) and exhibiting quasi-one-dimensional magnetic properties. In particular, we study fluorides containing these ions in a rarely encountered compressed octahedral coordination that forces the unpaired electron into the local $d(z^2)$ orbital. We predict that such systems should exhibit exchange anisotropies surpassing that of Sr_2CuO_3, one of the best realizations of a one-dimensional system known to date. In particular, we predict that the interchain coupling in the Ag^{2+}-containing $[AgF][BF_4]$ system should be nearly four orders of magnitude smaller than the intrachain interaction. Our results indicate that quasi-one-dimensional spin-$\frac{1}{2}$ systems containing chains with spin sites in the $d(z^2)^1$ local ground state could constitute a versatile model for testing modern theories of quantum many-body physics in the solid state.

DOI: 10.1103/PhysRevB.96.155140

I. INTRODUCTION

Coupling of structural, electronic, and magnetic degrees of freedom in compounds containing transition-metal cations with partially filled d shells leads to many intriguing phenomena, such as charge-density waves [1,2] or unconventional superconductivity [3,4]. Due to the strong Coulomb interaction within the d shell, such compounds are most often insulators [5], with the unpaired spin-density effectively localized on the transition-metal cations. In such systems magnetic interactions between the unpaired spins, which are mediated via the superexchange mechanism, can be described by the Heisenberg Hamiltonian

$$H = \sum_{i>j} J_{ij} \boldsymbol{S}_i \cdot \boldsymbol{S}_j, \tag{1}$$

where J_{ij} is the magnetic coupling constants between spin sites i and j. In this convention positive values of J_{ij} correspond to antiferromagnetic (AFM) spin ordering, while negative values correspond to a ferromagnetic (FM) spin ordering.

Much attention has been paid to the study of magnetic interactions in compounds containing Cu^{2+} cations ($3d^9$ electronic configuration), which are insulators and exhibit quasi-one-dimensional (quasi-1D) antiferromagnetic properties [6–10]. More recently, there has been an upsurge of interest in homologous systems featuring Ag^{2+} cations with a $4d^9$ electronic configuration [11–13]. In these compounds, which form regular 3D crystals, anisotropic superexchange between the unpaired electrons leads to a strong AFM interaction along one of the directions, with much weaker coupling along the other. As a result, these systems can be described as being composed of spin-$\frac{1}{2}$ Heisenberg chains characterized by an intrachain coupling constant J_{1D}, which can be defined by taking the Heisenberg Hamiltonian in the form given by Eq. (1) and considering only nearest neighbors along the chain:

$$H = J_{1D} \sum_i \boldsymbol{S}_i \cdot \boldsymbol{S}_{i+1}. \tag{2}$$

The ground state of a 1D AFM system composed of isolated chains is disordered (Luttinger liquid) [14,15]. This state is quantum critical, with very small interchain interactions (characterized by a coupling constant $J_\perp$) leading to three-dimensional magnetic ordering at finite Néel temperatures T_N [16–18]. However, even in the ordered state, the magnetic moments are extremely small due to quantum fluctuations [19]. Although 1D AFM systems have been intensely studied for more than half a century, new physical phenomena, such unusual magnetic excitations [20], are still being discovered.

Theoretical models of one-dimensional spin systems, such as those describing the spin transport mechanism [21,22], are best tested on systems characterized by large exchange anisotropies (i.e., low $|J_\perp|/J_{1D}$ ratios), which lead to very small ratios between the Néel temperature and the intrachain coupling constant. One of the best examples of such systems is Sr_2CuO_3, which exhibits T_N equal to 5.4 K [19] and $J_{1D} = 2785$ K [14,23], thus yielding a T_N/J_{1D} ratio of 1.9×10^{-3}. Recently we performed calculations of the intrachain coupling constant J_{1D} for a handful of quasi-1D AFM systems, including Sr_2CuO_3 [11]. We predicted that that $[AgF][BF_4]$, a compound containing Ag^{2+} cations, should exhibit J_{1D} equal to ∼3840 K, thus possibly surpassing in strength the AFM interactions exhibited by Sr_2CuO_3 and making it a good candidate for a model 1D AFM system, provided the interchain interactions are weak.

Following these findings, we present here calculations of relatively weak interchain coupling constants $J_\perp$ for a variety of Cu^{2+} and Ag^{2+} compounds exhibiting quasi-one-dimensional properties. By including some experimentally well-studied systems ($KCuF_3$, Sr_2CuO_3, Ca_2CuO_3, and $KAgF_3$), we verify that our method is capable of reproducing semiquantitatively the measured T_N/J_{1D} and $|J_\perp|/J_{1D}$ ratios. We confirm the 1D nature of $[AgF][BF_4]$ by predicting T_N/J_{1D} equal to 5.5×10^{-4} and single out other compounds that exhibit nearly ideal 1D AFM properties (i.e., low T_N/J_{1D} and $|J_\perp|/J_{1D}$ ratios). In particular, we find that several compounds containing Cu^{2+}/Ag^{2+} cations in a rare compressed octahedral geometry, which enforces single occupation of the $d(z^2)$ orbital, exhibit exchange anisotropies surpassing that of the

*d.kurzydlowski@cent.uw.edu.pl; w.grochala@cent.uw.edu.pl

presently best 1D AFM systems [all of which contain the unpaired electron in a $d(x^2-y^2)$ orbital].

In this work, by exchange anisotropy we refer to the different strength that magnetic interactions can have along bonds oriented in different directions (e.g., parallel vs perpendicular to chains). We do not take into account spin-orbit effects, which are relevant for anisotropy related to the orientations of the spins in space.

II. COMPUTATIONAL DETAILS

For each of the studied compounds we consider the nearest-neighbor interactions within the AFM-coupled chain J_{1D}, as well as diverse interchain interactions. All of the systems studied here are insulators with band gaps exceeding 1 eV. Depending on the structure of the compound, there might be more than one type of interchain coupling; in this case we will label those $J_{\perp}^{1}$, $J_{\perp}^{2}$, etc. For each type of superexchange coupling topology we present a complete analysis of all relevant superexchange interactions and derive models of magnetic states appropriate for the extraction of the interchain coupling constants.

Due to the single-determinant nature of density functional theory (DFT) calculations, we obtained the values of the coupling constants with the use of the broken-symmetry method [24,25]. We consider total energies of the system in a set of configurations with spins oriented along a particular axis (say z). Diagonal matrix elements of such configurations in Eq. (1) involve only the S_i^z and S_j^z operators and can be readily computed. For the detailed expressions used for the systems considered here, see Sec. III.

Solid-state collinear calculations were performed with the Heyd-Scuseria-Ernzerhof (HSE06) functional [26], which is a hybrid functional mixing the DFT generalized gradient approximation (GGA) functional of Perdew *et al.* [27], with 25% of the Hartree-Fock exchange energy. We found out previously that use of the HSE06 functional has led to a good reproduction of the intrachain superexchange coupling constants with a systematic and rather small 11% overestimation of their values [11]. Moreover, we note that the standard local density approximation and the GGA applied to the highly correlated systems studied here incorrectly predict a metallic or nearly metallic electronic ground state [28]. Although the use of DFT methods in strongly correlated systems may be dubious, hybrid functionals have been successfully applied in the study of low-dimensional magnets [11,28–30].

The projector-augmented-wave method [31,32] was used as implemented in the VASP 5.2 code [33–36]. Valence electrons were treated explicitly, while standard VASP pseudopotentials (accounting for scalar relativistic effects) were used for the description of core electrons. We used a plane-wave basis set with a cutoff energy of 920 eV, which was lowered to 850 eV for Cs- and Sr-containing compounds (Cs and Sr pseudopotentials do not allow for higher cutoff energies). The energy convergence criterion was 2×10^{-7} eV ($=2\times10^{-4}$ meV) per formula unit (f.u.). We used a fine k-point mesh with a spacing of $0.03\times2\pi$ Å^{-1}. The band energy was smeared with the use of the tetrahedron method with Blöchl corrections.

In our calculations we do not include noncollinear magnetic interactions. In the case of charge-transfer insulators studied here, such interactions are most often a result of spin-orbit coupling, which is small for d^9 ions in octahedral coordination due to orbital momentum quenching. In this work we focus on the relative strength of the inter- and intrachain interactions, which is mainly influenced by the strength of the superexchange interactions and not secondary spin-orbit coupling effects. In this approach we follow other works on quasi-1D AFM systems containing d^9 ions (e.g., on $KCuF_3$) [37].

Before performing single-point calculations to determine the values of the magnetic coupling constants, we optimized the geometry of every system by performing full relaxation of both the unit cell parameters and atomic coordinates. This optimization was conducted with the HSE06 functional and the parameters as given above. The convergence criteria for the relaxation were forces below 0.015 eV/Å and pressure below 1 kbar. The geometry optimization was conducted for the spin state of lowest energy (for a detailed comparison of the calculated and experimental geometries see Ref. [11]). We verified that the parameters employed in the calculations ensured convergence of the superexchange constants to within 2×10^{-3} meV (0.02 K). Visualization of structures and volumetric data has been performed with the use of the VESTA software [38].

III. RESULTS AND DISCUSSION

Due to the operation of the Jahn-Teller (JT) effect MX_6 complexes (the M d^9 cation and the X ligand) can exhibit either compressed or elongated octahedral geometry (D_{4h} symmetry). In the former scenario the underlying electronic state of the metal cation corresponds to half-occupation of the local $d(z^2)$ orbital of A_{1g} symmetry, while elongation forces the unpaired electron into the $d(x^2-y^2)$ orbital with B_{1g} symmetry (in both cases we define the local z axis as parallel to the axis of the JT distortion).

Based on the Goodenough-Anderson-Kanamori (GKA) rules [39–41], strong AFM coupling can be expected for chains composed of either (i) elongated MX_6 octahedra sharing two of the four equatorial (shorter) bonds or (ii) compressed MX_6 octahedra sharing both axial (shorter) bonds. Throughout this work we will describe the former structure motif, depicted in Fig. 1(a), as B_{1g} chains and the latter [Fig. 1(b)] as A_{1g} chains. Note that for A_{1g} chains the JT axis is parallel to the direction of the chain propagation, while for B_{1g} chains the JT distortion takes place in the perpendicular direction.

In this work we perform calculations for 15 oxides and fluorides containing Cu^{2+} and Ag^{2+} cations. For all of these systems the examination of the experimental crystal structure reveals that the M/F or M/O bonding network (M = Cu,Ag) can be described as composed of either B_{1g} or A_{1g} chains with the only deviation from Fig. 1 being that some of the systems exhibit nonlinear M-F-M or M-O-M bridges (the deviation from linearity does not exceed 60°). The two connectivity scenarios were identified by considering the topology of the short M–F or M–O bonds (i.e., bonds shorter than 2 Å for Cu^{2+} and 2.2 Å for Ag^{2+}). For systems exhibiting four short bonds (elongated octahedral), the resulting MF_4 squares are connected via opposing ligands thus forming chains; in the case of only two short bonds (compressed coordination) both bonds connect adjacent M^{2+} sites, which also results in the

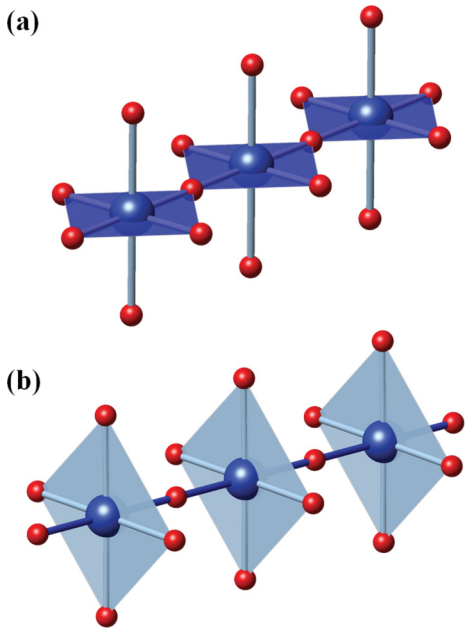

FIG. 1. (a) Arrangement of elongated MX_6 octahedral leading to formation of chains featuring half-occupation of the B_{1g} orbital of the M^{2+} cation. (b) Arrangement of compressed MX_6 octahedral leading to formation of chains featuring with half-occupied A_{1g} cation orbitals. Blue/red atoms balls depict M/X atoms; long/short M-X bonds are depicted with light blue/dark blue color.

formation of chains. In Sec. III we describe the properties of the systems studied, dividing them accordingly with respect to the ligand (fluorides and oxides) as well as to the structural features of the AFM-coupled chains (A_{1g}/B_{1g}).

We note that the structural motifs described above were treated only as a hint of possible 1D magnetic behavior. We term the compounds studied here quasi-one-dimensional because in all cases there is one dominant AFM superexchange route characterized by two nearest neighbors for each spin site; the J value for this superexchange route is at least an order of magnitude larger than any of the other coupling constants.

A. Fluorides with B_{1g} chains

We start our discussion with fluorides containing Cu^{2+} and Ag^{2+} cations with a general formula $M'MF_3$ (M' = Na,K,Rb, Cs,Ag; M = Cu,Ag). All of these compounds adopt structures that can be derived from the perovskite polytype. One of the most studied members of this family is $KCuF_3$, which is a prototypical quasi-1D AFM system [42–50].

This compound exhibits two polymorphs: a-$KCuF_3$ of $I4/mcm$ symmetry and d-$KCuF_3$ belonging to the $P4/mbm$ space group [43]. Due to orbital ordering first described by Kugel and Khomskii [51], both structures consist of B_{1g}-type chains separated by K^+ cations. The difference between the two polytypes lies in the relative orientation of CuF_4 plaquettes neighboring along the chain. As this feature does not markedly influence the superexchange interactions, we have conducted calculations for the larger unit cell polytype ($Z = 4$) a-$KCuF_3$, depicted in Fig. 2(a).

Due to the high symmetry of $KCuF_3$, there exists only one relevant interchain interaction $J_\perp$, shown in Fig. 2(b). Based

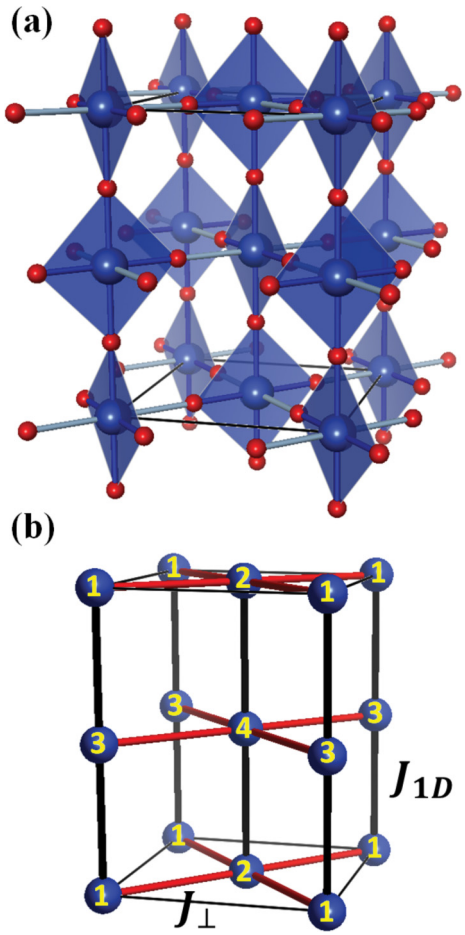

FIG. 2. (a) Structure of a-$KCuF_3$; K atoms were omitted for clarity. (b) Schematic description of the connectivity of the J_{1D} (black) and $J_\perp$ (red) superexchange paths.

on GKA rules, it is expected that the interchain coupling will be ferromagnetic, that is, $J_\perp < 0$. Indeed, the experimental value of $J_\perp$ is -21 K [52], while the intrachain coupling constant J_{1D} is equal to 406 K [44]. The nonzero interchain interaction leads to a finite Néel temperature of 39 K, hence $T_N/J_{1D} = 9.6\times10^{-2}$.

The value of the Néel temperature is dependent on the strength of both the inter- and intrachain coupling. Quantum Monte Carlo simulations on 1D AFM systems have enabled linking the value of the interchain interaction with T_N and J_{1D} for a 1D system

$$|J_\perp| = T_N \Big/ \left[4c\sqrt{\ln\left(\frac{\lambda J_{1D}}{T_N}\right) + \frac{1}{2}\ln\ln\left(\frac{\lambda J_{1D}}{T_N}\right)}\right], \quad (3)$$

where $c = 0.23$ and $\lambda = 2.6$ [18]. Inserting the experimental values of T_N and J_{1D} determined for $KCuF_3$ into Eq. (3) yields $|J_\perp|$ equal to 20.9 K, in very good agreement with the experimental value.

In order to extract magnetic coupling constants with the use of the broken-symmetry method we have constructed three spin states of a-$KCuF_3$: (i) the $F1$ state with intra- and interchain FM coupling, (ii) the $A1$ state with AFM coupling within chains and FM coupling between them, and (iii) the $A2$ state with AFM coupling along both superexchange routes.

TABLE I. Magnetic states of $KCuF_3$. Spin up/down sites are indicated with a $+/-$ sign. Site labeling follows that of Fig. 2(b). Here E_{nm} denotes the part of the total energy of the system, which is independent of the spin state.

	Site				
State	1	2	3	4	Energy per f.u.
$F1$	+	+	+	+	$0.25J_{1D} + 0.5J_{\perp} + E_{nm}$
$A1$	+	+	−	−	$-0.25J_{1D} + 0.5J_{\perp} + E_{nm}$
$A2$	+	−	+	−	$-0.25J_{1D} - 0.5J_{\perp} + E_{nm}$

The formulas linking the energy of these spin states with J_{1D} and $J_{\perp}$ are summarized in Table I together with the direction of the unpaired spins on each Cu^{2+} site of the $KCuF_3$ crystal structure [Fig. 2(b)]. The formulas from Table I can be combined to extract the superexchange constants

$$J_{1D} = 2F1 - 2A1, \tag{4}$$

$$J_{\perp} = A1 - A2. \tag{5}$$

By calculating the energies of the $F1$, $A1$, and $A2$ magnetic states with the use of the HSE06 hybrid functional we obtain the J_{1D} and $J_{\perp}$ values of 594 and −48 K, respectively. These values are comparable to those obtained in the previous periodic calculations of Moreira *et al.*, which employed the B3LYP hybrid functional ($J_{1D} = 652$ K and $J_{\perp} = -23.2$ K) [29].

With the theoretical values of J_{1D} and $J_{\perp}$ we can obtain the value of T_N with the use of Eq. (3) and hence calculate the T_N/J_{1D} ratio. For $KCuF_3$ we obtain in our calculations $T_N/J_{1D} = 14\times10^{-2}$, which is rather close to the experimental value of 9.6×10^{-2} (taking theoretical values reported in Ref. [30], one arrives at $T_N/J_{1D} = 6.9\times10^{-2}$). The overestimation in our calculations of the experimental T_N/J_{1D} ratio can be traced back to the overestimation of the $|J_{\perp}|/J_{1D}$ ratio (a theoretical value of 8.1×10^{-2} compared to the 5.2×10^{-2} derived from experiment).

For other perovskite fluorides of copper and silver the inter- and intrachain couplings can be extracted by the same procedure as for $KCuF_3$. Apart from $CsAgF_3$, which is isostructural with a-$KCuF_3$ [53], the structure of these compounds ($KAgF_3$ [12], $RbAgF_3$ [53], and $NaCuF_3$/$AgCuF_3$ [54]) can be derived from that of a-$KCuF_3$ by introduction of tilting of the MX_6 octahedra [55]. This distortion, however, does not alter the topology of the superexchange pathways and therefore the spin states given in Table I can be used to extract J_{1D} and $J_{\perp}$ through Eqs. (4) and (5). In Table II we report the calculated values of $J_{\perp}$ together with the values of $|J_{\perp}|/J_{1D}$ and T_N/J_{1D}.

Although magnetic susceptibility of $CsAgF_3$ and $RbAgF_3$ was measured [53], the values of T_N and J_{1D} were not determined for these systems. Our calculations agree well with the experimental data of $KAgF_3$ with T_N/J_{1D} slightly overestimated compared to the experimental one. The largest discrepancy between theory and experiment is found for $AgCuF_3$ and $NaAgF_3$. Taking the experimental ordering temperatures and intrachain coupling constants of these systems [54], one arrives at T_N/J_{1D} ratios considerably lower than the theoretical ones. However, the magnetic ordering temperatures

TABLE II. Values of the magnetic coupling constants and the $|J_{\perp}|/|J_{1D}|$ and T_N/J_{1D} ratios calculated for fluorides of divalent copper and silver exhibiting B_{1g} chains. The values of J_{1D}, previously reported in Ref. [11], were obtained with the same computational method as used in this work. Theoretical T_N values were calculated from $J_{\perp}$ and J_{1D} using Eq. (3). Experimental data, in parentheses, for $KCuF_3$ [44,52], $AgCuF_3$/$NaCuF_3$ [54], and $KAgF_3$ [12] are given for comparison. Here ND denotes not determined.

System	J_{1D} (K)	$J_{\perp}$ (K)	$\lvert J_{\perp}\rvert/J_{1D}(10^{-3})$	$T_N/J_{1D}(10^{-3})$
$KCuF_3$	594 (406)	−48 (–21)	81 (52)	140 (96)
$AgCuF_3$	436 (298)	−61 (ND)	140 (ND)	222 (67)
$NaCuF_3$	369 (191)	−59 (ND)	160 (ND)	249 (94)
$CsAgF_3$	1867 (ND)	−106 (ND)	57 (ND)	103 (ND)
$RbAgF_3$	1669 (ND)	−83 (ND)	49 (ND)	92 (ND)
$KAgF_3$	1311 (1160)	−58 (ND)	44 (ND)	82 (57)

of $AgCuF_3$ and $NaCuF_3$ were derived from susceptibility measurements of samples containing FM impurities. The authors took T_N as the temperature corresponding to a peak in the magnetic susceptibility, but this peak is found in the region where the signal from FM impurities is dominant. It thus possible that long-range magnetic order sets out at higher temperatures than those initially presumed [54], but remains masked by the Curie-like temperature dependence of the impurities. In this case the experimental T_N/J_{1D} values would be higher than reported and thus closer to our theoretical values.

Comparing the $|J_{\perp}|/J_{1D}$ ratios calculated for Ag(II) fluorides and Cu(II) fluorides shows that the former compounds exhibit larger exchange anisotropies, despite being characterized by stronger interchain FM coupling. This is mostly a consequence of the much stronger intrachain AFM interactions. This feature in turn originates from a much more pronounced hybridization of the Ag($4d$) states with F($2p$) than that taking place for the Cu($3d$) and F($2p$) states [56].

B. Oxides with B_{1g} chains

We now turn to two oxide systems containing Cu^{2+} cations in an elongated octahedral coordination, Sr_2CuO_3 and Ca_2CuO_3. Both compounds are considered as one of the best realizations of a quasi-1D AFM-coupled system among all inorganic compounds and they constitute important references in our quest for model 1D AFM systems [57,58]. Their structure, depicted in Fig. 3(a), consists of B_{1g}-type chains with linear Cu-O-Cu bridges [59,60].

We distinguish two interchain superexchange paths, which are depicted in Fig. 3(b). The shorter one is $J_{\perp}^1$ and it links the AFM-coupled chains into 2D sheets. Given the fact that ideal 2D systems do not display long-range order at finite temperatures, one must also include another superexchange path that couples the 2D sheets. Therefore, a longer route, characterized by the $J_{\perp}^2$ coupling constant, is also taken into account in our model. Both $J_{\perp}^1$ and $J_{\perp}^2$ can be combined into an effective interchain coupling constant $J_{\perp}^{\text{eff}}$,

$$|J_{\perp}^{\text{eff}}| = \frac{\sum_n z_n |J_{\perp}^n|}{\sum_n z_n}, \tag{6}$$

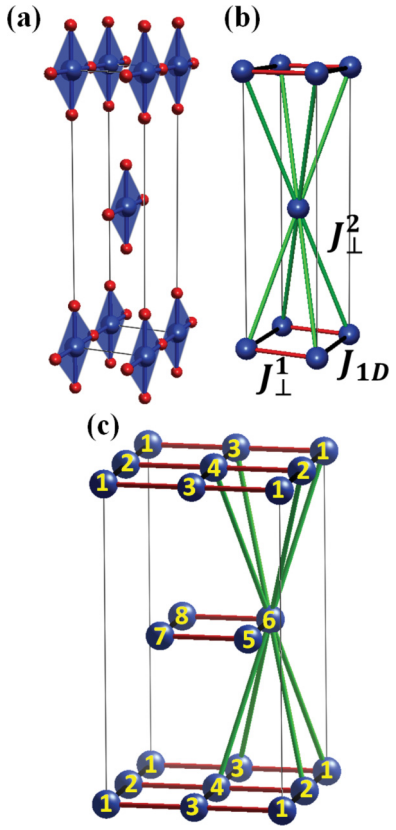

FIG. 3. (a) Structure of M'_2CuO_3 (M' = Ca,Sr); M' atoms were omitted for clarity. (b) Schematic description of the connectivity of the J_{1D} (black line), $J_\perp^1$ (red line), and $J_\perp^2$ (green line) superexchange paths. (c) The 1×2×2 supercell used for the calculation of the coupling constants.

where z_n is the number of neighbors along a given interchain exchange coupling route (for M'_2CuO_3 with $z_1 = 4$ and $z_2 = 8$). The effective interchain interaction can be used together with the value of J_{1D} to predict the value of T_N through Eq. (3).

In order to calculate the three magnetic coupling constants (J_{1D}, $J_\perp^1$, and $J_\perp^2$) four spin states have to be taken into account; these are described in Table III. Apart from $F1$, all of these states require extending the structure of $M'CuO_3$ into a 1×1×2 supercell and therefore all calculations were performed in this supercell, which is depicted in Fig. 3(c).

Equations (7)–(9) give the values of the coupling constants with respect to the magnetic states

$$J_{1D} = F1 - 2A1 + A3, \quad (7)$$

$$J_\perp^1 = F1 - 2A2 + A3, \quad (8)$$

$$J_\perp^2 = 0.5F1 - 0.5A3. \quad (9)$$

The calculated values of the coupling constants are summarized in Table IV. The interaction along the $J_\perp^1$ superexchange route is weakly antiferromagnetic, in accord with previous calculations of de Graaf and Illas [30]. This AFM coupling is most probably a result of the space interaction between $d(x^2-y^2)$ orbitals of neighboring chains. This notion is further corroborated by the fact that $J_\perp^1$ is larger for Ca_2CuO_3, which exhibits shorter interchain separations than its Sr analog [60].

TABLE III. Magnetic states of M'_2CuO_3 (M' = Sr,Ca). Spin up/down sites are indicated with a +/− sign; their labeling follows that of Fig. 3(c).

	Site								
State	1	2	3	4	5	6	7	8	Energy per f.u.
$F1$	+	+	+	+	+	+	+	+	$0.25J_{1D} + 0.25J_\perp^1 + J_\perp^2 + E_{nm}$
$A1$	+	−	+	−	+	−	+	−	$-0.25J_{1D} + 0.25J_\perp^1 + E_{nm}$
$A2$	+	+	−	−	+	+	−	−	$0.25J_{1D} - 0.25J_\perp^1 + E_{nm}$
$A3$	+	+	+	+	−	−	−	−	$0.25J_{1D} + 0.25J_\perp^1 - J_\perp^2 + E_{nm}$

Analogous weak AFM interactions are observed in $CuCl_2 \cdot 2H_2O$ [61], as well as Na_2AgF_4 [13], both of which exhibit similar stacking of plaquettes containing spin-$\frac{1}{2}$ cations.

As in the case of $KCuF_3$ and $KAgF_3$, we observe quite good accord between our calculations and the experimental values of $|J_\perp^{eff}|/J_{1D}$ and T_N/J_{1D}, with both ratios slightly overestimated in the calculations (see Table IV). Unfortunately, there are no oxide systems of divalent silver with which M'_2CuO_3 compounds can be compared. This is a result of the strong tendency towards disproportionation of Ag^{2+} to diamagnetic Ag^+ and low-spin Ag^{3+} in the oxide environment, which cannot be reversed even under application of high pressure [62].

C. Fluorides with A_{1g} chains

Although axial elongation is more commonly found than compression for d^9 systems with deformed octahedral coordination [63–67], there are several systems containing Cu^{2+} and Ag^{2+} cations in the genuine local A_{1g} ground state [i.e., with half-occupation of the local $d(z^2)$ orbital of the metal]. Among these $[MF][AsF_6]$ (M = Cu,Ag), $M'CuAlF_5$ (M' = K,Cs), and $CsAgAlF_6$ adopt structures containing A_{1g} chains with bent M-F-M bridges [68–72]. As shown in the Supplemental Material [73], these systems exhibit the same topology of the superexchange paths as $KCuF_3$. Consequently, spin states described in Table I can be used for the extraction of the intra- and interchain coupling constants via Eqs. (4) and (5). The results of the calculations are summarized in Table V.

The magnetic ordering temperatures for the A_{1g} fluorides studied were not determined [although for Cu^{2+}-containing compounds they lie below 6 K (see Ref. [71])] and therefore no comparison can be made between our results and the experimental ones. It is noteworthy to point, however, to the extremely small value of T_N/J_{1D} (comparable to or even lower than that of M'_2CuO_3) found for this group of compounds.

Apart from the compounds mentioned above, there are two more important fluoride systems exhibiting A_{1g} chains, namely, [CuF][AuF_4] [74] and [AgF][BF_4] [70], which both contain linear M-F-M bridges. Both are magnetically dense systems, with many relatively short secondary $M\cdots M$ separations and a complex topology, and therefore the correct description of the interactions between the AFM chains requires taking into account more than one interchain coupling pathway.

At ambient conditions [CuF][AuF_4] crystallizes in a monoclinic cell containing A_{1g} chains separated by AuF_4^- units [Fig. 4(a)]. To account for all of the shortest interchain

TABLE IV. Values of the magnetic coupling constants and the $|J_\perp^{\rm eff}|/J_{1D}$ and T_N/J_{1D} ratios calculated for $M_2'CuO_3$. The values of J_{1D}, previously reported in Ref. [11], were obtained with the same computational method as used in this work. Theoretical T_N values were calculated from $J_\perp$ and J_{1D} using Eq. (3). The experimental $|J_\perp^{\rm eff}|/J_{1D}$ ratio (given in parentheses) was estimated from experimental J_{1D} and T_N values (Sr_2CuO_3 [19,23] and Ca_2CuO_3 [57]) using Eq. (3). In the case of Ca_2CuO_3 we assumed $J_{1D} = 2680$ K as derived from rigorous configuration-interaction calculations [30]. Here ND denotes not determined.

System	J_{1D} (K)	$J_\perp^1$ (K)	$J_\perp^2$(K)	$\lvert J_\perp^{\rm eff}\rvert$ (K)	$\lvert J_\perp^{\rm eff}\rvert/J_{1D}(10^{-3})$	$T_N/J_{1D}(10^{-3})$
Sr_2CuO_3	3058 (2797)	17	−0.4	3.8	1.3 (0.7)	3.2 (1.9)
Ca_2CuO_3	2961 (ND)	24	2.1	6.5	2.2 (1.6)	5.4 (4.1)

interactions we include in our model three interchain couplings, as shown in Fig. 4(b). In order to extract the J values at least five spin states have to be constructed within a 2×2×2 supercell [73].

The tetragonal structure of [AgF][BF_4] can be described as containing A_{1g} chains (with linear and nearly symmetric Ag-F-Ag bridges) linked by BF_4^- tetrahedra [Fig. 5(a)]. Apart from the intrachain coupling constant there are three relevant interchain exchange routes [Fig. 5(b)]. The spin states and their relation to the coupling constant values are given in Ref. [73].

For both [CuF][AuF_4] and [AgF][BF_4] an effective interchain interaction can be defined using Eq. (6), with $z_1 = z_2 = z_3 = 2$ for the former compound and $z_1 = z_2 = z_3 = 4$ for the latter. As in the case of $M_2'CuO_3$, we use the value of $|J_\perp^{\rm eff}|$ together with J_{1D} to obtain the magnetic ordering temperature and consequently T_N/J_{1D}. The results, summarized in Table VI, indicate that although both compounds are characterized by interchain interactions of similar strength, [AgF][BF_4] is a better realization of a 1D AFM system than [CuF][AuF_4] as a result of a stronger intrachain coupling [11].

D. Next-nearest-neighbor interactions within chains

For strongly-AFM-coupled systems, interactions beyond nearest neighbors might be significant, as exemplified by the ring exchange observed in the 2D AFM systems La_2CuO_4 [75,76]. We therefore consider the next-nearest-neighbor (NNN) coupling along the chains ($J_{1D}^{\rm NNN}$) for five selected quasi-1D AFM systems. The common feature of these systems is that they exhibit linear M-F-M and M-O-M bridges and hence the strongest AFM coupling in the respective compound families [11]. We choose systems with the largest J_{1D} values, as we assume that $J_{1D}^{\rm NNN}$ will be smaller than the nearest-neighbor interaction by an order of magnitude or more. Hence it will be relevant only for systems exhibiting large-J_{1D} values; this assumption is correct, as shown below.

In order to extract the value of $J_{1D}^{\rm NNN}$, a magnetic state with paired spins (P state in Fig. 6) has to be taken into account. For this state contributions from nearest-neighbor interactions cancel out, while the contribution from the NNN coupling is $-1/4J_{1D}^{\rm NNN}$ per spin site. For chains characterized by both FM and AFM order, taking the NNN interaction into account shifts the energy by $+1/4J_{1D}^{\rm NNN}$ per spin site. Consequently, the value of $J_{1D}^{\rm NNN}$ can be calculated through the following expression:

$$J_{1D}^{\rm NNN} = FM + AFM - 2P. \quad (10)$$

The values of the NNN coupling, summarized in Table VII, are sizable for systems exhibiting strong nearest-neighbor

TABLE V. Values of the magnetic coupling constants and the $|J_\perp|/|J_{1D}|$ and T_N/J_{1D} ratios calculated for fluorides of divalent copper and silver exhibiting A_{1g} chains. The values of J_{1D}, previously reported in Ref. [11], were obtained with the same computational method as used in this work. Theoretical T_N values were calculated from $J_\perp$ and J_{1D} using Eq. (3).

System	J_{1D} (K)	$J_\perp$ (K)	$\lvert J_\perp\rvert/J_{1D}(10^{-3})$	$T_N/J_{1D}(10^{-3})$
[CuF][AsF_6]	404	0.5	1.3	3.4
$CsCuAlF_6$	292	0.1	0.3	0.8
$KCuAlF_6$	162	−0.1	0.8	2.2
[AgF][AsF_6]	1418	−5.1	3.6	8.5
$CsAgAlF_6$	670	−0.6	0.9	2.5

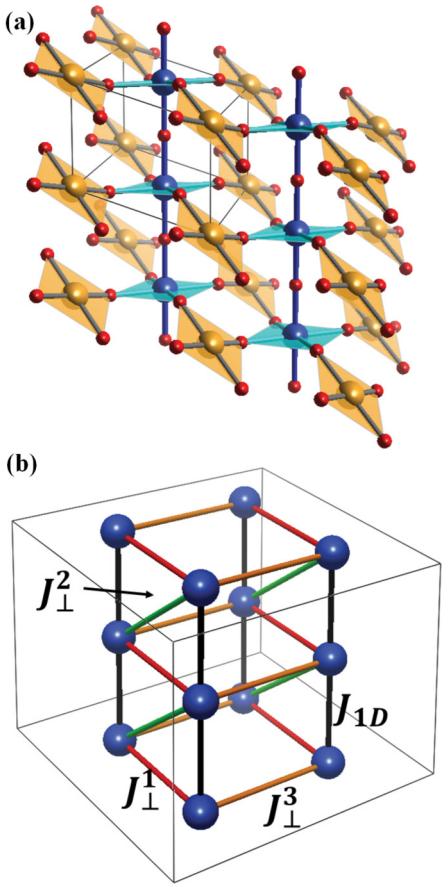

FIG. 4. (a) Structure of [CuF][AuF_4] with gold atoms marked as orange balls. (b) The 2×2×2 supercell used for calculations of magnetic coupling constants, together with the depiction of the superexchange paths.

TABLE VI. Values of the magnetic coupling constants and the $|J_\perp^{\rm eff}|/J_{\rm 1D}$ and $T_N/J_{\rm 1D}$ ratios calculated for [CuF][AuF_4] and [AgF][BF_4]. The values of $J_{\rm 1D}$, previously reported in Ref. [11], were obtained with the same computational method as used in this work. Theoretical T_N values were calculated from $J_\perp$ and $J_{\rm 1D}$ using Eq. (3).

System	$J_{\rm 1D}$ (K)	$J_\perp^1$ (K)	$J_\perp^2$ (K)	$J_\perp^3$ (K)	$\lvert J_\perp^{\rm eff}\rvert$ (K)	$\lvert J_\perp^{\rm eff}\rvert/J_{\rm 1D}(10^{-3})$	$T_N/J_{\rm 1D}(10^{-3})$
[CuF][AuF_4]	862	−0.3	2.1	−2.7	1.7	2	4.9
[AgF][BF_4]	3843	−0.4	−0.1	1.6	0.7	0.2	0.6

interaction ([AgF][BF_4], $CsAgF_3$, and Sr_2CuO_3). The ratio between $J_{\rm 1D}^{\rm NNN}$ and $J_{\rm 1D}$ does not exceed 6×10^{-2}, similarly to La_2CuO_4 for which the ratio between NN and NNN interactions within the [CuO_2] sheets was determined experimentally to of an order of 1.5×10^{-2} [75]. The predicted positive sign of both $J_{\rm 1D}^{\rm NNN}$ and $J_{\rm 1D}$ hints at a possible weak spin frustration within the chains featured in both [AgF][BF_4] and Sr_2CuO_3, due to the second-nearest-neighbor intrachain coupling. Additional calculations conducted for $KAgF_3$ and $RbAgF_3$, which exhibit bent Ag-F-Ag bridges but still sizeable $J_{\rm 1D}$ values (see Table II), also lead to $|J_{\rm 1D}^{\rm NNN}|/|J_{\rm 1D}|$ ratios of an order of 10^{-2} (see Ref. [73]).

E. Summary

In order to assess the accuracy of the HSE06 functional for prediction of the inherently weak interchain superexchange, we compare the experimentally known $T_N/J_{\rm 1D}$ ratios with those calculated here. As follows from Fig. 7, there exists a linear relationship between theoretical and experimental results, with the former being usually overestimated by (45.3 ± 0.4)%. The error is larger for $AgCuF_3$ and $NaCuF_3$, for which, however, there are doubts about the true value of their magnetic ordering temperatures (see Sec. III A). The semiquantitative agreement between calculated end experimental $T_N/J_{\rm 1D}$ ratios is encouraging given their small values ($10^{-1}-10^{-3}$); it should be noted that direct differences between theoretical and experimental values range from 4.4×10^{-2} for $KCuF_3$ to 1.3×10^{-3} for Sr_2CuO_3. As mentioned earlier the overestimation of $T_N/J_{\rm 1D}$ can be traced back to the overestimation of the $|J_\perp^{\rm eff}|/J_{\rm 1D}$ ratio. That is, the strength of the weak interchain couplings, most of them ferromagnetic, is more overestimated in our calculations than in the intrachain AFM interactions, for which an 11% overestimation is found [11].

The good agreement between theoretical and experimental data justifies the comparison between the whole set of studied structures, including those for which T_N and $J_{\rm 1D}$ are not established. A summary of the calculated $T_N/J_{\rm 1D}$ and $|J_\perp^{\rm eff}|/J_{\rm 1D}$ ratios, given in Fig. 8, shows that among the studied compounds four exhibit exchange anisotropies larger than that of Sr_2CuO_3. Moreover, all of these systems exhibit A_{1g}-type chains containing either Cu^{2+} ($CsCuAlF_6$ and $KCuAlF_6$), or Ag^{2+} cations ([AgF][BF_4] and $CsAgAlF_6$).

In particular, [AgF][BF_4] is characterized by a calculated $|J_\perp^{\rm eff}|/J_{\rm 1D}$ ratio of only 1.9×10^{-4} and the resulting computed $T_N/J_{\rm 1D}$ ratio is equal to 5.5×10^{-4}. These values are close to those estimated from experiment for DEOCC-$TCNQF_4$ (0.2×10^{-4} and 0.6×10^{-4}, respectively, for $|J_\perp^{\rm eff}|/J_{\rm 1D}$ and the scaled Néel temperature), an organic radical-ion salt claimed as the best known realization of an 1D AFM system [52]. Indeed, the moderate value of the intrachain coupling constant

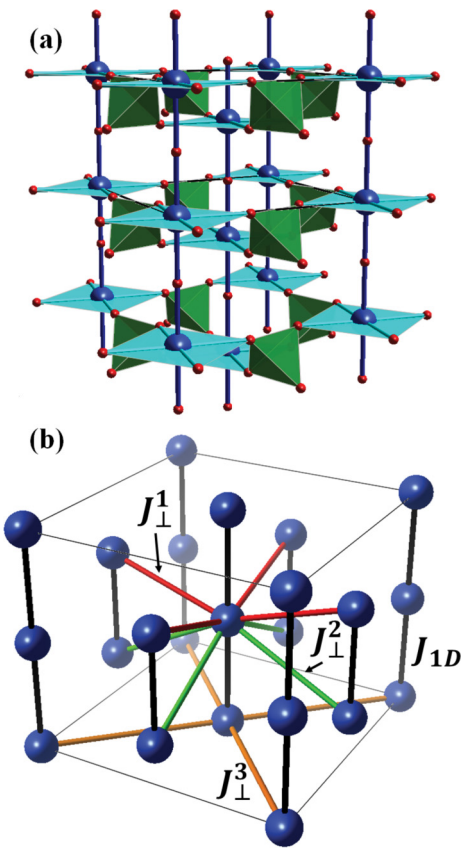

FIG. 5. (a) Structure of [AgF][BF_4] with BF_4^- anions marked as green tetrahedra. (b) The $\sqrt{2}\times\sqrt{2}\times2$ supercell used for calculations of magnetic coupling constants, together with the depiction of the superexchange paths.

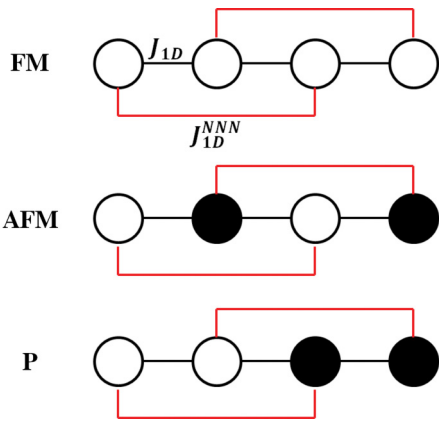

FIG. 6. Depiction of the magnetic states used for calculations of $J_{\rm 1D}^{\rm NNN}$. Open/closed balls depict spin-up/spin-down sites.

TABLE VII. Values of next-nearest-neighbor intrachain interactions (J_{1D}^{NNN}) calculated for selected systems exhibiting linear superexchange pathways.

System	J_{1D}^{NNN} (K)	$\lvert J_{1D}^{NNN}\rvert/\lvert J_{1D}\rvert(10^{-2})$
$[AgF][BF_4]$	228	5.9
$CsAgF_3$	54	2.9
Sr_2CuO_3	148	4.8
$[CuF][AuF_4]$	7	0.9
$KCuF_3$	0.2	0.04

of DEOCC-TCNQF$_4$ (110 K) results in a very low Néel temperature, with 3D magnetic order not detectable even at 20 mK [52]. In contrast, we predict that $[AgF][BF_4]$ should exhibit a magnetic ordering temperature of about 2 K, although we note that our calculations do not take into account noncollinear interactions (e.g., the Dzyaloshinsky-Moriya coupling), as well as possible frustration of interchain interactions, both of which can influence the value of the magnetic ordering temperature for this compound (as well as for the $M_2'CuO_3$ reference systems) [77,78]. However, more importantly, the extremely strong AFM intrachain interaction found for $[AgF][BF_4]$ (J_{1D} exceeding 3000 K) should enable testing the spin dynamics of this system even at temperatures above the magnetic ordering, similarly to the case of Sr_2CuO_3. In view of these results, experimental examination of magnetic features of $[AgF][BF_4]$ certainly constitutes an interesting goal.

For the studied compounds we find that systems exhibiting A_{1g} chains are generally characterized by larger exchange anisotropies (i.e., lower $|J_{\perp}^{eff}|/J_{1D}$ ratio) than B_{1g} systems,

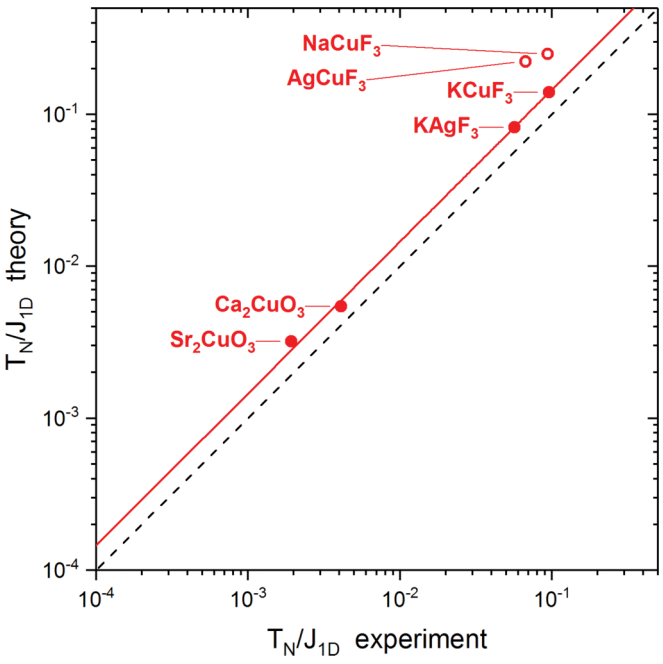

FIG. 7. Comparison of experimental and theoretical values of the T_N/J_{1D} ratios for compounds that feature the unpaired electron in the $d(x^2-y^2)$ orbital of a metal. The red line marks a linear regression passing through (0,0) with a slope of 1.453 ± 0.004. The values for $AgCuF_3$ and $NaCuF_3$, not included in the fit, are shown by open symbols.

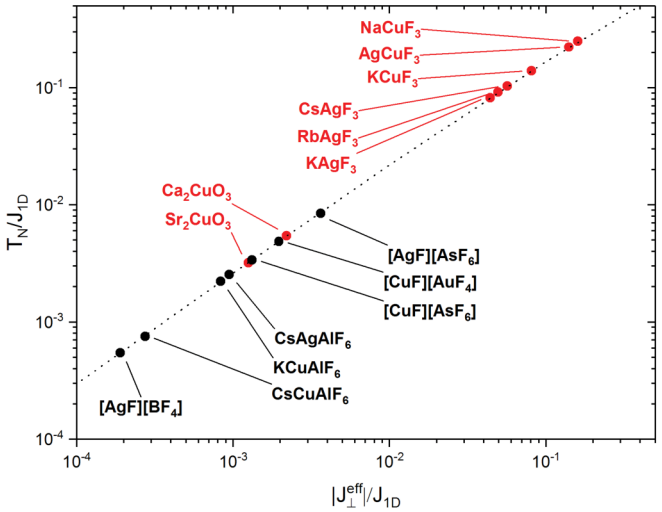

FIG. 8. Calculated dependence of the Néel temperature scaled by $J_{1D}(T_N/J_{1D})$ as a function of $|J_{\perp}^{eff}|/J_{1D}$. Systems with A_{1g} chains are marked in black, those exhibiting B_{1g} chains in red. The dotted line represents the dependence given by Eq. (3).

as evident from Fig. 8. There are several reasons behind this. One is that chains built of compressed Cu^{2+}/Ag^{2+} octahedra lead to stronger AFM intrachain interactions than those seen for elongated octahedra [11]. Second, most of the A_{1g} systems studied here have M^{2+} concentrations smaller than the corresponding B_{1g} compounds and this greater dilution of spin sites leads to weaker interchain interactions. However, we find that for $[AgF][BF_4]$ the exchange anisotropy remains high even upon volume reduction due to application of high pressure [79,80] up to 100 kbars (see Ref. [73]).

The exchange anisotropy observed in all of the compounds studied is a direct consequence of the orbital ordering, which is largely connected with the cooperative Jahn-Teller effect. Since the work of Kugel and Khomskii [51], it was debated whether superexchange-mediated orbital ordering proposed by these authors drives a collective distortion of the Jahn-Teller ions or it is the elastic interaction (electron-phonon coupling) of locally distorted d^9 complexes that dictates the structure and hence electronic configuration of the compound. A study of $KCuF_3$ by Pavarini *et al.* indicated that both Jahn-Teller distortions and the superexchange mechanism need to be invoked in order to explain the persistence of orbital order in this compound up to 800 K [81]. Estimation of the relative importance of the two orbital order mechanisms for the wide range of compounds studied here is certainly interesting, although beyond the scope of the current work, especially since other investigations pointed to the important role of long-range interactions [66,82] and tilting distortions [83] in promoting orbital ordering and importantly indicated the limitation of the orbital ordering approach [84]. Given the fact that Ag(II)/F systems exhibit a very strong Jahn-Teller effect even for isolated ions [85,86], one might speculate that electron-phonon coupling will be a major driving force for orbital ordering in those systems.

Finally, we note that although our calculations do not take account of spin-orbit coupling, the great majority of systems studied by us are centrosymmetric and obviously the unpaired electron resides on either the local $d(x^2-y^2)$ (B_{1g} systems) or

$d(z^2)$ (A_{1g}) orbital. In such a case the spin-orbit effects cancel in the first approximation [87].

IV. CONCLUSION

We performed hybrid density functional calculations of magnetic coupling constants for a variety of quasi-1D AFM systems. Our calculations reproduced with good accuracy the experimental T_N/J_{1D} ratio. Importantly, we found that fluoride systems containing Ag^{2+} and Cu^{2+} cations in compressed octahedral coordination should constitute a novel family of quasi-1D systems exhibiting strong intrachain AFM coupling and simultaneously very weak interchain coupling. For example, we showed that for [AgF][BF_4] the computed values of $|J_{\perp}^{\mathrm{eff}}|/J_{1D}$ and T_N/J_{1D} are equal to 1.9×10^{-4} and 5.5×10^{-4}, respectively; these values are smaller by approximately one order of magnitude than the calculated values for well researched Sr_2CuO_3. Hence, [AgF][BF_4] might be one of the best realizations of a quasi-1D AFM system. Importantly, this compound and other members of this group feature d^9 Ag^{2+}/Cu^{2+} cations with one unpaired electron occupying the local $d(z^2)$ orbital rather than the $d(x^2-y^2)$ one (as found for Sr_2CuO_3).

We hope that this study will motivate experimental investigation into the properties of [AgF][BF_4] and its siblings, in particular in the context of novel phenomena that might arise from the different local symmetry of the spin-carrying orbital. Future studies might also extend the theoretical description of the systems presented here, especially by examining in detail the origin of orbital ordering observed in the A_{1g} chains, as well as addressing the issue of secondary spin-orbit coupling effects. We note, however, that the latter calculations are extremely CPU consuming and therefore might not be feasible for all of the compounds studied, at least at the hybrid DFT level employed in this work.

ACKNOWLEDGMENTS

W.G. thanks the National Science Centre of the Republic of Poland for HARMONIA Grant No. 2012/06/M/ST5/00344 and ICM UW for time at OKEANOS supercomputer (ADVANCE Plus, GA67-13). Comments from Professor José Lorenzana and Dr. M. Derzsi are greatly appreciated. We are also grateful to Professor Bogumił Jeziorski for the many years of inspiration.

[1] T. Kloss, X. Montiel, V. S. de Carvalho, H. Freire, and C. Pépin, Rep. Prog. Phys. **79**, 84507 (2016).
[2] C.-W. Chen, J. Choe, and E. Morosan, Rep. Prog. Phys. **79**, 84505 (2016).
[3] D. J. Scalapino, Rev. Mod. Phys. **84**, 1383 (2012).
[4] N. M. Plakida, Physica C **531**, 39 (2016).
[5] J. Zaanen, G. Sawatzky, and J. Allen, Phys. Rev. Lett. **55**, 418 (1985).
[6] K. Katsumata, Curr. Opin. Solid State Mater. Sci. **2**, 226 (1997).
[7] S. J. Blundell, Contemp. Phys. **48**, 275 (2007).
[8] L. J. de Jongh and A. R. Miedema, Adv. Phys. **23**, 1 (1974).
[9] A. Tressaud and J.-M. Dance, Struct. Bond. **52**, 87 (1982).
[10] K. S. Pedersen, M. A. Sørensen, and J. Bendix, Coord. Chem. Rev. **299**, 1 (2015).
[11] D. Kurzydłowski and W. Grochala, Angew. Chem. Int. Ed. **56**, 10114 (2017).
[12] D. Kurzydłowski, Z. Mazej, Z. Jagličić, Y. Filinchuk, and W. Grochala, Chem. Commun. **49**, 6262 (2013).
[13] D. Kurzydłowski, Z. Mazej, and W. Grochala, Dalton Trans. **42**, 2167 (2013).
[14] A. C. Walters, T. G. Perring, J.-S. Caux, A. T. Savici, G. D. Gu, C.-C. Lee, W. Ku, and I. A. Zaliznyak, Nat. Phys. **5**, 867 (2009).
[15] B. Lake, A. M. Tsvelik, S. Notbohm, D. A. Tennant, T. G. Perring, M. Reehuis, C. Sekar, G. Krabbes, and B. Büchner, Nat. Phys. **6**, 50 (2010).
[16] V. Y. Irkhin and A. A. Katanin, Phys. Rev. B **61**, 6757 (2000).
[17] M. Bocquet, Phys. Rev. B **65**, 184415 (2002).
[18] C. Yasuda, S. Todo, K. Hukushima, F. Alet, M. Keller, M. Troyer, and H. Takayama, Phys. Rev. Lett. **94**, 217201 (2005).
[19] K. Kojima, Y. Fudamoto, M. Larkin, G. Luke, J. Merrin, B. Nachumi, Y. Uemura, N. Motoyama, H. Eisaki, S. Uchida, K. Yamada, Y. Endoh, S. Hosoya, B. Sternlieb, and G. Shirane, Phys. Rev. Lett. **78**, 1787 (1997).
[20] E. G. Sergeicheva, S. S. Sosin, L. A. Prozorova, G. D. Gu, and I. A. Zaliznyak, Phys. Rev. B **95**, 020411 (2017).
[21] J. Sirker, R. G. Pereira, and I. Affleck, Phys. Rev. Lett. **103**, 216602 (2009).
[22] R. Steinigeweg and W. Brenig, Phys. Rev. Lett. **107**, 250602 (2011).
[23] J. Lorenzana and R. Eder, Phys. Rev. B **55**, R3358 (1997).
[24] M.-H. Whangbo, K. Hyun-Joo, and D. Dai, J. Solid State Chem. **176**, 417 (2003).
[25] F. Illas, I. D. P. R. Moreira, C. de Graaf, and V. Barone, Theor. Chem. Acc. **104**, 265 (2000).
[26] A. V. Krukau, O. A. Vydrov, A. F. Izmaylov, and G. E. Scuseria, J. Chem. Phys. **125**, 224106 (2006).
[27] J. P. Perdew, K. Burke, and M. Ernzerhof, Phys. Rev. Lett. **77**, 3865 (1996).
[28] P. Rivero, I. D. P. R. Moreira, and F. Illas, Phys. Rev. B **81**, 205123 (2010).
[29] I. D. P. R. Moreira and R. Dovesi, Int. J. Quantum Chem. **99**, 805 (2004).
[30] C. de Graaf and F. Illas, Phys. Rev. B **63**, 014404 (2000).
[31] P. E. Blöchl, Phys. Rev. B **50**, 17953 (1994).
[32] G. Kresse and D. Joubert, Phys. Rev. B **59**, 1758 (1999).
[33] G. Kresse and J. Hafner, Phys. Rev. B **47**, 558 (1993).
[34] G. Kresse and J. Hafner, Phys. Rev. B **49**, 14251 (1994).
[35] G. Kresse and J. Furthmüller, Phys. Rev. B **54**, 11169 (1996).
[36] G. Kresse and J. Furthmüller, Comput. Mater. Sci. **6**, 15 (1996).
[37] M. D. Towler, R. Dovesi, and V. R. Saunders, Phys. Rev. B **52**, 10150 (1995).
[38] K. Momma and F. Izumi, J. Appl. Crystallogr. **41**, 653 (2008).
[39] J. B. Goodenough, *Magnetism and the Chemical Bond* (Interscience, New York, 1963).
[40] P. W. Anderson, Solid State Phys. **14**, 99 (1963).
[41] J. Kanamori, J. Phys. Chem. Solids **10**, 87 (1959).
[42] S. Kadota, I. Yamada, S. Yoneyama, and K. Hirakawa, J. Phys. Soc. Jpn. **23**, 751 (1967).
[43] N. Tsukuda and A. Okazaki, J. Phys. Soc. Jpn. **33**, 1088 (1972).

[44] S. Satija, J. Axe, G. Shirane, H. Yoshizawa, and K. Hirakawa, Phys. Rev. B **21**, 2001 (1980).

[45] D. A. Tennant, S. E. Nagler, D. Welz, G. Shirane, and K. Yamada, Phys. Rev. B **52**, 13381 (1995).

[46] B. Lake, D. A. Tennant, and S. E. Nagler, Phys. Rev. Lett. **85**, 832 (2000).

[47] B. Lake, D. A. Tennant, and S. E. Nagler, Phys. Rev. B **71**, 134412 (2005).

[48] B. Lake, D. A. Tennant, C. D. Frost, and S. E. Nagler, Nat. Mater. **4**, 329 (2005).

[49] J. Deisenhofer, I. Leonov, M. V. Eremin, C. Kant, P. Ghigna, F. Mayr, V. V. Iglamov, V. I. Anisimov, and D. van der Marel, Phys. Rev. Lett. **101**, 157406 (2008).

[50] J. Deisenhofer, M. Schmidt, Z. Wang, C. Kant, F. Mayr, F. Schrettle, H.-A. Krug von Nidda, P. Ghigna, V. Tsurkan, and A. Loidl, Ann. Phys. (Leipzig) **523**, 645 (2011).

[51] K. I. Kugel and D. I. Khomskii, Zh. Eksp. Teor. Fiz. **64**, 1429 (1973) [Sov. Phys. JETP **37**, 725 (1973)].

[52] F. L. Pratt, S. J. Blundell, T. Lancaster, C. Baines, and S. Takagi, Phys. Rev. Lett. **96**, 247203 (2006).

[53] R.-H. Odenthal and R. Hoppe, Monatsh. Chem. **102**, 1340 (1971).

[54] J. Tong, C. Lee, M.-H. Whangbo, R. K. Kremer, A. Simon, and J. Köhler, Solid State Sci. **12**, 680 (2010).

[55] M. W. Lufaso and P. M. Woodward, Acta Crystallogr. B **60**, 10 (2004).

[56] W. Grochala, R. G. Egdell, P. P. Edwards, Z. Mazej, and B. Žemva, Chem. Phys. Chem. **4**, 997 (2003).

[57] A. Keren, K. Kojima, L. P. Le, G. M. Luke, W. D. Wu, Y. J. Uemura, S. Tajima, and S. Uchida, J. Magn. Magn. Mater. **140–144**, 1641 (1995).

[58] N. Motoyama, H. Eisaki, and S. Uchida, Phys. Rev. Lett. **76**, 3212 (1996).

[59] N. C. Hyatt, L. Gray, I. Gameson, P. P. Edwards, and S. Hull, Phys. Rev. B **70**, 214101 (2004).

[60] M. Hjorth, J. Hyldtoft, A. Mostad, C. Rømming, R. Salmén, H. H. Tønnesen, and T. Tokii, Acta Chem. Scand. **44**, 516 (1990).

[61] W. Marshall, J. Phys. Chem. Solids **7**, 159 (1958).

[62] A. Grzelak, J. Gawraczyński, T. Jaroń, M. Somayazulu, M. Derzsi, V. Struzhkin, and W. Grochala, Inorg. Chem. **56**, 5804 (2017).

[63] M. A. Halcrow, Chem. Soc. Rev. **42**, 1784 (2013).

[64] D. Kurzydłowski, M. Derzsi, Z. Mazej, and W. Grochala, Dalton Trans. **45**, 16255 (2016).

[65] F. Rodríguez, Inorg. Chem. **56**, 2029 (2017).

[66] J. A. Aramburu, P. García-Fernández, J. M. García-Lastra, and M. Moreno, J. Phys. Chem. C **121**, 5215 (2017).

[67] S. V. Streltsov and D. I. Khomskii, Phys. Rev. B **89**, 201115 (2014).

[68] B. G. Müller, J. Fluor. Chem. **17**, 317 (1981).

[69] G. Wingefeld and R. Hoppe, Z. Anorg. Allg. Chem. **516**, 223 (1984).

[70] W. J. Casteel, G. M. Lucier, R. Hagiwara, H. Borrmann, and N. Bartlett, J. Solid State Chem. **96**, 84 (1992).

[71] Z. Mazej, I. Arčon, P. Benkič, A. Kodre, and A. Tressaud, Chem. Eur. J. **10**, 5052 (2004).

[72] M. Atanasov, M. A. Hitchman, R. Hoppe, K. S. Murray, B. Moubaraki, D. Reinen, and H. Stratemeier, Inorg. Chem. **32**, 3397 (1993).

[73] See Supplemental Material at http://link.aps.org/supplemental/10.1103/PhysRevB.96.155140 for (i) structures of fluorides containing A_{1g} chains, (ii) magnetic states of [CuF][AuF_4]/[AgF][BF_4], (iii) the pressure dependence of the $|J_{\perp}^{\mathrm{eff}}|/J_{1\mathrm{D}}$ and $T_N/J_{1\mathrm{D}}$ ratios for [AgF][BF_4], and (iv) values of next-nearest-neighbor intrachain interactions calculated for $M\mathrm{AgF_3}$ compounds.

[74] B. G. Müller, Angew. Chem., Int. Ed. **26**, 688 (1987).

[75] R. Coldea, S. M. Hayden, F. Aguado, T. G. Perring, C. D. Frost, T. E. Mason, S.-W. Cheong, and Z. Fisk, Phys. Rev. Lett. **86**, 5377 (2001).

[76] J. Lorenzana, J. Eroles, and S. Sorella, Phys. Rev. Lett. **83**, 5122 (1999).

[77] M. Hälg, W. E. A. Lorenz, K. Y. Povarov, M. Månsson, Y. Skourski, and A. Zheludev, Phys. Rev. B **90**, 174413 (2014).

[78] Z. Z. Du, H. M. Liu, Y. L. Xie, Q. H. Wang, and J.-M. Liu, Phys. Rev. B **94**, 134416 (2016).

[79] S. Haravifard, D. Graf, A. E. Feiguin, C. D. Batista, J. C. Lang, D. M. Silevitch, G. Srajer, B. D. Gaulin, H. A. Dabkowska, and T. F. Rosenbaum, Nat. Commun. **7**, 11956 (2016).

[80] K. R. O'Neal, B. S. Holinsworth, Z. Chen, P. K. Peterson, K. E. Carreiro, C. Lee, J. L. Manson, M.-H. Whangbo, Z. Li, Z. Liu, and J. L. Musfeldt, Inorg. Chem. **55**, 12172 (2016).

[81] E. Pavarini, E. Koch, and A. I. Lichtenstein, Phys. Rev. Lett. **101**, 266405 (2008).

[82] H. Wu, C. F. Chang, O. Schumann, Z. Hu, J. C. Cezar, T. Burnus, N. Hollmann, N. B. Brookes, A. Tanaka, M. Braden, L. H. Tjeng, and D. I. Khomskii, Phys. Rev. B **84**, 155126 (2011).

[83] E. Pavarini, S. Biermann, A. Poteryaev, A. I. Lichtenstein, A. Georges, and O. K. Andersen, Phys. Rev. Lett. **92**, 176403 (2004).

[84] V. Polinger, in *The Jahn-Teller Effect*, edited by H. Köppel, D. Yarkony, and H. Barentzen, Springer Series in Chemical Physics Vol. 97 (Springer, Berlin, 2009), pp. 685–725.

[85] P. García-Fernández, A. Trueba, M. T. Barriuso, J. A. Aramburu, and M. Moreno, Phys. Rev. Lett. **104**, 035901 (2010).

[86] Z. Mazej, D. Kurzydłowski, and W. Grochala, in *Photonic and Electronic Properties of Fluoride Materials*, edited by A. Tressaud and K. Poeppelmeier (Elsevier, Amsterdam, 2016), pp. 231–260.

[87] K. I. Kugel and D. I. Khomskii, Sov. Phys. Usp. **25**, 231 (1982).